Two-Phase Mini-Thermosyphon Electronics Cooling, Part 1: Experimental Investigation

Chin Lee Ong, Nicolas Lamaison, Jackson B. Marcinichen and John R.Thome*
Heat and Mass Transfer Laboratory (LTCM)
Ecole Polytechnique Fédérale de Lausanne (EPFL)
EPFL STI IGM LTCM / EL H0 094 / Station 9 CH-1015
Lausanne, Switzerland
Email: john.thome@epfl.ch

ABSTRACT

Efficient, small, state-of-the-art passive cooling two-phase systems, i.e. advanced micro-thermosyphon cooling systems, are viable solutions for high performance datacenter servers and power electronics cooling applications. The objective of this study is to push through the "two-phase threshold" that seems to be hindering the application of this cooling technology by offering here proven experimental results (Part 1), validated steady-state and transient simulation tools (Parts 2 and 3) and a server case study (Part 4). The experimental investigation in Part 1 presents the thermal-hydraulic performance of a mini-thermosyphon loop with a small riser height, H_{riser} = 15.0 cm. The thermosyphon loop has a multi-microchannel copper evaporator, mounted on top of a pseudo-chip CPU emulator (heat source). Experimental results for R134a, acquired under both pumped flow and passive thermosyphon driven flow (for direct comparison) for mass flow rates up to 10 kg/hr, uniform heat fluxes, q of up to 61.4 W/cm^2 and refrigerant filling ratios up to 83% were obtained. An innovative thermal calibration method, developed as a non-intrusive mass flow measurement technique, has also been implemented to monitor the thermosyphon's operation. Summarizing in brief, the two-phase thermosyphon loop with an integrated in-line liquid accumulator offered a very sustainable cooling performance for the microchannel/pseudo-CPU package, and is a first step forward in our effort towards the integration of such two-phase passive cooling devices for data center servers and other electronic devices at heat flux of up to 80 W/cm^2 (or more).

KEY WORDS:

Two-phase, passive cooling, thermosyphon, electronics cooling.

NOMENCLATURE

A	current, ampere
G	mass flux, kg/m^{2}s
H	height, cm
L	length, cm
$\dot{m}$	mass flow rate, kg/hr
q	heat flux, W/cm^2, kW/m^2
T	temperature, ^{o}C
x	vapor quality, -

Greek symbols

ΔP	pressure difference, Pa
ΔV	voltage drop, V
ε	void fraction, -
Ω	resistance, ohms
ρ	density, kg/m^3

Subscripts

cond	condenser
conv	convective
crit	critical
d,c	downcomer
frict	frictional
h	homogeneous
in	inlet
l	liquid
ref	refrigerant
sat	saturation
sub	sub-cooling
th	thermal
tsp	thermosyphon
v	vapor

Acronyms

CB	coalescing bubble
CRAH	computer room air handler
CPU	central processing unit
FDR	frictional dominant regime
FR	filling ratio
GDR	gravity dominant regime
IB	isolated bubble
IT	information technology

INTRODUCTION

The paradigm shift from performance-driven to efficient computing is creating a demand for more innovative and efficient cooling concepts to minimize power consumption and cooling costs for ownership of data centers. Efficient cooling of IT equipment still remains a major challenge for most thermal and electronics design engineers today and the most economically viable solution is currently still being debated. This concerns strategies that exhibit the best combination of high cooling effectiveness, compact thermal designs, low thermo-mechanical stresses induced on the chip, no or low vibrations by the cooling system to the server, low cost and low energy consumption, reliability and scalability.

Cooling strategies for datacenter servers have evolved during the past decade, moving from air cooled architectures to water cooled systems. For example, 28 CRAHs were deployed to cool 126 racks (3400 kW) in 2005, 2 CRAHs for 12 racks (864 kW) with 80% water cooling in 2008 and one 100% water

cooled rack (175 kW) in 2011 [1]. Water-cooled systems at the chip level are simple and demonstrate efficient heat transfer characteristics, allowing computational and power density to be increased. However, water based cooling systems are primarily single-phase, which are more practical for low heat flux conditions without hot spots. High inlet-outlet chip temperature gradients (due to the coolant temperature rise across the chip) induce additional thermal stress on the chip and TIM, thereby reducing reliability. Water based systems also require periodic control of fluid resistivity, pH, corrosion inhibitors and biocides to prevent biofouling of the cold plates. In addition, flow induced vibrations from a pumped water loop (or fans for air cooling) can reach and pose operational issues for data storage devices integrated into servers, which then throttle down their read/write speeds by 50% or more, greatly reducing server throughput. Simply, this either means twice as many servers are needed for the job or twice as much time to do it, both resulting in much higher energy operating costs for the job to get done.

Passive two-phase mini-thermosyphon cooling loops eliminate use of mechanically rotating (vibrating) components while employing dielectric fluids as coolants (R134a presently). These passive heat transfer devices rely only on the buoyancy forces due to the fluid density differences between the two-phase riser and the liquid downcomer as the driving force for coolant circulation into an evaporator, yielding much higher flow rates and thus higher heat dissipation rates than the capillary flow in heat pipes. Minimal fluid inlet sub-cooling and a low pressure drop across the evaporator enhance temperature uniformity (intrinsic characteristic of evaporative cooling), which are highly desirable to ensure optimum operational efficiency of the cooled electronics. The compactness of mini-thermosyphon loops also reap the additional benefit of a near isothermal system, optimizing exergetic efficiency due to a very low temperature/pressure drop within the loop. Furthermore, thermosyphon loops are increasingly being deployed for the cooling of power electronics [2,3] and for fuel cell thermal management [4]. Marcinichen et al. [5] demonstrated the feasibility of integrating a mini-thermosyphon cooling loop into a blade server as part of the effort towards the development of passively cooled datacenters. Simulation results concluded that a very compact thermosyphon loop is absolutely feasible and can guarantee high chip temperature uniformity even under transient heat flux disturbances and an absence of dryout condition even with the presence of hot spots.

Part 1 presents the experimental characterization of a mini-thermosyphon cooling system for 2U height servers (but also applicable to vertically oriented blades and miniservers). The primary objective is to experimentally validate the thermal performance of a mini-thermosyphon cooling loop with a small riser height, H_{riser} = 15.0 cm, noting that this is taller than a 2U since non-intrusive integrated thermosyphon flow rate measurements are integrated for simulation code benchmarking purposes. In fact, steady-state and transient experimental data acquired during the experimental campaign are used to validate our in-house simulation tool in Parts 2 and 3, and then used to design a mini-thermosyphon cooling device suitable for the cooling of a 2U server in Part 4.

STATE-OF-THE-ART REVIEW

Selected publications relating to the characterization of close loop thermosyphon systems performance, with respect to the coolant used, heat load, coolant charge (filling ratio, FR) and condenser air flow rate or cooling air temperature on the system pressure are reviewed below.

Agostini et al. [2] studied a compact thermosyphon cooler with R134a and H_{riser} = 40.0 cm with an integrated air-cooled condenser. In their study, it was concluded that an optimum refrigerant charge yielded the lowest total thermal resistance, FR ~ 0.48 in their case, where the dependency of thermal resistance on FR was due to two competing effects, namely, (i) higher evaporator thermal resistance for low FRs because of local dryout due to liquid deficiency and (ii) condenser flooding at higher FRs. The effect of the air temperature (system saturation pressure) was also investigated, with the conclusion that the thermal resistances for both the evaporator and condenser at higher air temperatures rise due to lower buoyancy driving force when going up to T_{sat} = 83 ºC (T_{crit} = 101ºC). The experimental study of Garrity et al. [4] with HFE-7100 as the coolant identified a mass flow rate variation trend with respect to heat flux. Their experimental mass flow measurements indicated an increasing mass flow rate at low heat fluxes, reaching a maximum flow rate at q = 24 kW/m^2 before a decreasing trend was observed at higher heat fluxes before encountering the onset of a Ledinegg instability at q = 32 kW/m^2. The experimental findings of Na et al. [6] with R11 and HCFC-123 for various types of cooling modules concurred with the findings of [4], observing similar mass flow rate-heat flux trends. An increasing trend was observed for low heat flux conditions, encountering a peak mass flow rate at q = 5kW/m^2 before witnessing a declining mass flow rate at higher heat flux conditions. They also observed that the effective convective thermal resistance decreased linearly with increasing heat flux. Furthermore, they documented that the system performance is highly dependent on the appropriate condenser size and FR.

Chang et al. [7] characterized their mini closed loop thermosyphon device for various FRs, i.e. 0.03, 0.07, 0.27, 0.47 and 0.67 with water as the working fluid and reached the following conclusions: (i) lower evaporator and condenser thermal resistance for higher heat fluxes are due to increased flow within the thermosyphon loop, (ii) higher condenser thermal resistance at higher FRs is due to the rise in condenser pressure and compressed vapor and (iii) larger temperature oscillations were observed for lower FRs of 0.27, and 0.47 but were dampened out for the highest FR ~ 0.67. Tsoi et al. [8] carried out investigation on thermosyphon test plates under horizontal and vertical orientation for water under sub-atmospheric conditions and values of FR ~ 0.22 - 0.32. Their experimental results also indicated lower thermal resistance at higher FRs and elevated heat flux conditions. They also concluded that favorable gravitational orientation enhanced circulation in their vertical thermosyphon test plate, thus resulting in consistently better thermal characteristics in comparison with the horizontal orientation.

Franco et al. [9] experimentally characterized a closed loop thermosyphon with L_{riser} = 75 cm and $L_{d,c}$ = 120 cm with water and ethanol as the coolants. Experimentally measured mass flow rate trends were similar to observations in [4], i.e. an

increasing and decreasing mass flow rate trend with heat flux. In general, they also validated that higher mass flow rates were realized for higher FR and lower system pressure conditions. Thus, the maximum mass attainable flow rate was highly dependent on the system pressure and FR.

Summarizing all this work, a number of conclusions were drawn for the thermal resistance with respect to mass flow rate, heat flux, FRs and system pressure: (i) the mass flow rate was identified to be dependent on the imposed heat flux, where according to Bieliński et al. [10], the mass flow rate within a thermosyphon close loop can be subdivided into two regimes, namely the gravity dominant regime (GDR) and the frictional dominant regime (FDR). In the GDR, a small change in vapor quality induces a larger void fraction whereby the liquid-vapor density gradient induces a large buoyancy force and thus higher driving potential for flow circulation whilst a large rise in vapor quality is accompanied with a substantial increase in frictional pressure drop that explains the decreasing trend in mass flow rate at higher heat fluxes in the FDR flow regime, (ii) in two-phase flow, flow boiling heat transfer improves with increasing heat flux whereby its thermal resistance decreases with heat flux (more specifically in the IB/CB flow regime) and mass flux. This explains the lower thermal resistances reported in literature for higher heat flux conditions in the GDR. In the FDR, there is a competing effect whereby the lower thermal resistance due to elevated heat flux is compensated by a reduction in mass flow rate. The experimental data of Agostini et al. [2] for FR ~ 0.50 showed significant evaporator thermal resistance reduction at lower heat flux conditions, reaching a trough followed by a marginally higher resistance at higher heat fluxes as opposed to observations reported in [6-9], (iii) FR was identified as an important parameter that affects the thermal performance of the evaporator, and hence the entire thermosyphon cooling loop. Undercharging of the thermosyphon loop results in occasional liquid dryout in the evaporator [2] while overcharging eventually results in condenser flooding. In general, an optimum charge without condenser flooding should yield higher mass flow rates due to a higher driving potential, i.e. larger liquid height in the downcomer section of the thermosyphon loop. This illustrates that the optimum FR is greatly dependent on the condenser and downcomer volumes; that is a high condenser volume fraction (V_{cond}/V_{tsp}) will yield a lower FR if condenser flooding is to be avoided.

EXPERIMENTAL CAMPAIGN

A mini-thermosyphon loop has been constructed to experimentally characterize its thermal performance as shown in Fig. 1. The thermosyphon loop comprises a copper microchannel evaporator, an inclined riser section with a sight glass for flow visualization purposes, an inclined water cooled condenser, a 25 cm^3 liquid accumulator, a stainless steel heater for mass flow rate measurements and a 3-way valve for switching between the pump or closed thermosyphon loop operation. The evaporator is mounted on a PCB board equipped with a heater that emulates the heat source from a CPU. The heater was manufactured by Delphi Corporation (know as a PST1-02/5PU Thermal Test Die) comprising an array of 35 heaters, arranged 5 in the flow-wise and 7 in the lateral-wise direction. Each individual heater is 2.54 mm x 2.54 mm in dimension and is equipped with a resistance diode sensor of 25Ω, 24.2V and 0.8A. The total pseudo-chip thickness, width and length are respectively 350 µm, 17.78 mm and 12.7 mm. A high thermal conductivity liquid metal alloy TIM (62.5%Ga - 21.5%In - 16.0%Sn) of thickness ~ 40 µm was applied between the evaporator and thermal test chip. Absolute and differential pressure transducers were installed at the evaporator inlet/outlet plenum to measure local inlet saturation pressure and evaporator pressure drop. Calibrated type-K thermocouples to within ±0.08 K uncertainty were positioned along the thermosyphon and condenser water loop to measure the local fluid temperatures.

The microchannel evaporator was comprised of 52 channels, each 163 µm and 1660 µm height and average fin thickness of 178 µm. The total evaporator width and length were 17.78 mm and 15.6 mm respectively while the copper base below the channels was 1.8 mm in thickness. A tube-in-tube condenser (Danfoss – HE 0.5) was installed at a -2.6º inclination to facilitate liquid drainage into the downcomer. The condensing refrigerant flows in the inner tube while cooling water flows counter current in the annulus. The thermosyphon loop dimensions and components are reported in Table 1.

Sections	*Dimensions*
Accumulator	25.0 cm^3
Riser length, L_{riser}	40.9 cm
Riser height, H_{riser}	15.0 cm
Condenser	17.8 cm
Downcomer length, $L_{d,c}$	112.0 cm
L_{heater}	15.0 cm
d_{heater}	4.0 cm
d_{riser} and $d_{d,c}$	4.7 cm

Table 1: Thermosyphon section component dimensions.

The experimental campaign under thermosyphon mode was carried out for two configurations, i.e. with and without the accumulator. Isolating the in-line accumulator by closing the two bypass valves connected to the accumulator leads to a smaller closed loop volume whereby the liquid that is drained from the condenser flows directly into the downcomer. Opening the accumulator bypass valves and shutting the downcomer loop valve (installed parallel to the accumulator) prescribes liquid drainage from the condenser outlet into the accumulator. All experimental test runs with mass flow measurements requires the isolation of the accumulator to generate enough sub-cooling and prevent boiling in the flow rate calibration heater. This means the refrigerant exiting the condenser flows directly into the downcomer and is drawn into the microchannel evaporator. This operating mode (isolated accumulator) presents some limitations, especially for higher condenser water temperatures, i.e. T_{water} > 20 ºC or for lower water flow rates, $\dot{m}_{water}$ < 8 kg/hr. Under these conditions, insufficient condenser cooling was encountered, meaning saturated two-phase flow was drawn into the downcomer and evaporator. This resulted in significant micro-evaporator inlet pressure and chip temperature oscillations. Under these circumstances, experimental test runs could not reach steady operation. The series of tests was then repeated with the inclusion of the in-line

accumulator. The presence of the accumulator guaranteed the creation of a stratified liquid pool at the bottom of the accumulator, which is then drawn into the downcomer and evaporator. Temperature and pressure stability in the micro-evaporator was thus maintained for the entire experimental test range, including T_{water} temperatures of up to 40 °C and $\dot{m}_{water}$ as low as ~ 4 kg/hr.

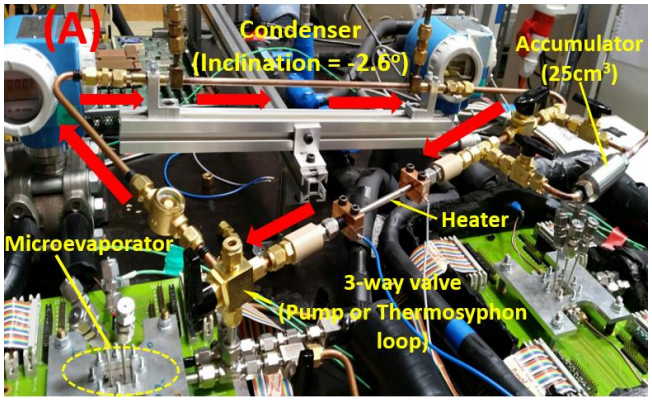

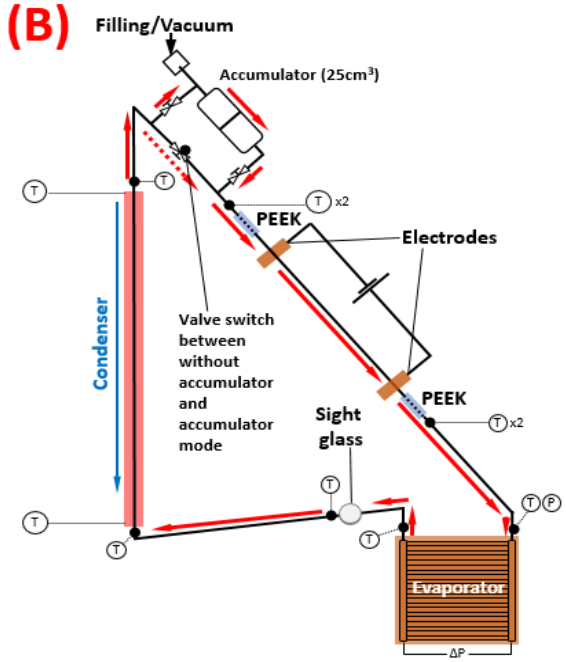

Fig. 1 (A) Experimental mini-thermosyphon test loop (condenser replaced with Danfoss HE 0.5) and (B) Schematic diagram of the thermosyphon loop.

Thermal mass flow rate calibration procedure

A thermal mass flow rate measurement technique has been implemented on the thermosyphon loop as illustrated in Figure 1. This technique employs a stainless steel heater connected to a pair of copper electrodes for low power electrical heating (Agilent DC power supply N5745A-30V/25A, 750W). Voltage drop measurements across the stainless steel heater were carried out with multimeter, model no. HP 34401A. Two pairs of type-K thermocouples (4 in total) were positioned at insulated locations along the heater to measure the local liquid temperature rise. A reference mass flow meter, i.e. Coriolis flow meter (EMERSON Micro Motion Elite – CMF010M323 1700R11 MVD) was used to measure the actual mass flow rate during the calibration process using a gear pump to drive the subcooled refrigerant in the loop during the calibration process. The procedure is as follows:

The refrigerant loop is filled with a refrigerant charge, i.e. 520 g and 525 g (to demonstrate that the measured flow results are unaffected by refrigerant charge).

i) A small heat load of ~ 0.96 W (ΔV = 0.194 V, I = 4.88 A) is imposed on the heater and the fluid temperature rise and the mass flow rate are then acquired.
ii) Measurements were carried out for a range of mass flow rates from 3 – 12 kg/hr, with a step increment of 1 kg/hr per acquisition.
iii) Applying an energy balance of the heater to the liquid flow, the experimental data were then fitted to yield a 2nd degree polynomial to the deduced mass flow rates use for the thermosyphon experiments (see Fig. 2).

The fitted polynomial shown in below can then be used to deduce the thermosyphon experimental mass flow rate (acquired without the accumulator) with an uncertainty of ± 8% without disturbing the loop's hydraulic flow resistance.

$$\dot{m} = 39.100903\Delta T^2 - 49.216147\Delta T + 18.401206 \quad (1)$$

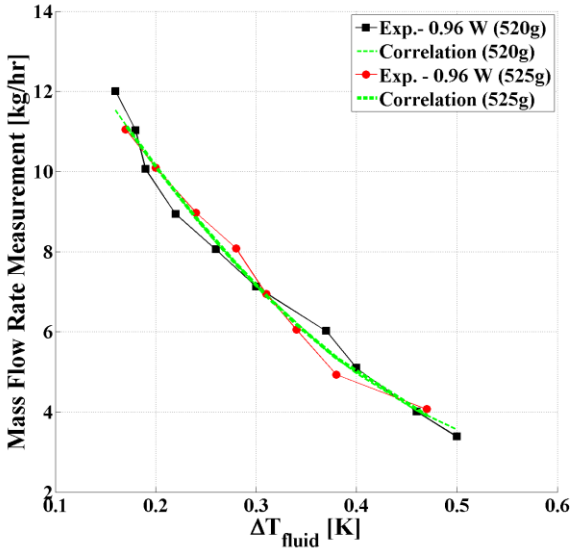

Fig. 2 Experimental mass flow rate calibration results and curve fitting.

EXPERIMENTAL RESULTS

Thermosyphon refrigerant mass flow rate

Figure 3 illustrates the experimental mass flow rates measured for FR's of 0.76 and 0.83 at two water mass flow rates of 8 and 10 kg/hr. The first observable trend is the increasing mass flow rate at low heat flux up to 30 W/cm^2, before observing a significant decrease in mass flow rate at q > 30 W/cm^2 ($\dot{m}_{water}$ = 8 kg/hr). These trends can be attributed to the gravity dominant regime (GDR) and frictional dominant regime (FDR) discussed earlier. The second trend relates to the filling ratio (FR) whereby a higher thermosyphon mass flow rate was

recorded for at the higher FR ~ 0.83. This is not surprising as it is consistent with experimental data from other studies. Physically speaking, as the FR increased, the liquid height in the downcomer increased, thus yielding a higher driving potential within the loop. This is similarly true for data obtained under higher cooling water mass flow rates, i.e. $\dot{m}_{water}$ = 10 kg/hr and FR ~ 0.76 for q < 25 W/cm^2. For higher cooling water mass flow rates, a lower thermosyphon loop pressure can be expected and this results in a higher liquid-vapor density difference, i.e. higher driving potential for this gravity dominated regime.

The driving potential in a thermosyphon loop is dependent on the void fraction ε in the riser. A small variation in evaporator exit quality yields a large change in the void fraction and larger density difference with respect to the liquid in the downcomer, giving rise to a significantly higher driving potential, $\Delta P_{driving}$ as illustrated according to:

$$\Delta P_{driving} = (\rho_l - \rho_h) g H_{d,c} \quad (2)$$

where, ρ_h is the homogeneous density evaluated based on vapor quality, x and the homogeneous void fraction equation, ε_h:

$$\rho_h = \rho_l(1 - \varepsilon_h) + \rho_v \varepsilon_h \quad (3)$$

$$\varepsilon_h = \frac{1}{1 + \left(S \frac{(1-x)}{x} \frac{\rho_v}{\rho_l}\right)} \quad (4)$$

A slip ratio of S = 1 for homogenous flow was used in the simulation presented in Figure 4.

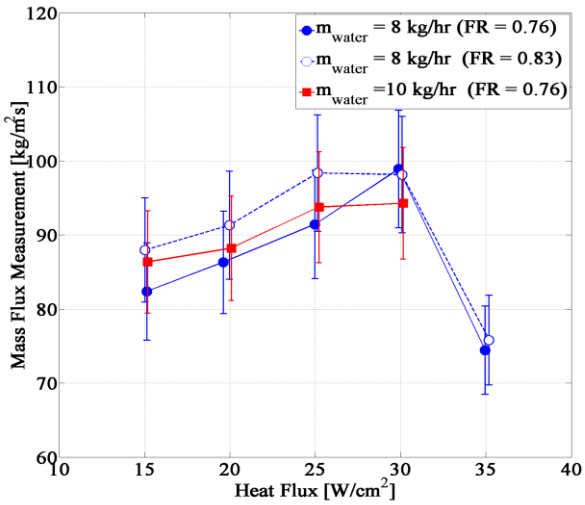

Fig. 3 Experimental mass flux measurement (without accumulator) for $T_{water,in}$ = 12 °C.

The net driving potential is thus defined as:

$$\Delta P_{net,driving} = \Delta P_{driving} - \Delta P_{fric,riser} - \Delta P_{cond} - \Delta P_{d,c} \quad (5)$$

where ΔP_{fric} is the homogeneous frictional pressure drop evaluated based on the Cicchitti two-phase viscosity relation defined as:

$$\mu_{tp} = x\mu_v + (1 - x)\mu_l \quad (6)$$

Figure 4 illustrates net driving potential simulation (excluding the pressure drop in the condenser and single-phase frictional pressure loss in the downcomer) for different saturation temperatures/pressures as a function of heat flux. In this comparison, the net driving potential is highest for the lowest saturation temperature/pressure and a drop in net driving potential is observable for the higher saturation temperatures. According to the simulation results, the peak mass flow rate occurred at q ~ 30 W/cm^2 (T_{sat} = 12 °C), q ~ 40 W/cm^2 (T_{sat} = 20 °C) and q ~ 60 W/cm^2 (T_{sat} = 30°C), respectively.

At elevated heat fluxes, the net driving potential decreases due to the dominance of frictional losses. This trend is observed to be more pronounced for the T_{sat} = 12 and 20 °C while becoming steadier at higher saturation temperatures for the range of simulated heat flux. For comparison, the net driving potential for T_{sat} = 12 °C intersect T_{sat} = 20 °C at q ~ 60 W/cm^2. In reality, this intersection point will shift towards lower heat fluxes when pressure loss in the condenser and downcomer is taken into account. This decreasing trend explains the lower refrigerant mass flow rate trend at q > 30 W/cm^2 for $\dot{m}_{water}$ = 10 kg/hr (FR ~ 0.76) shown in Figure 3.

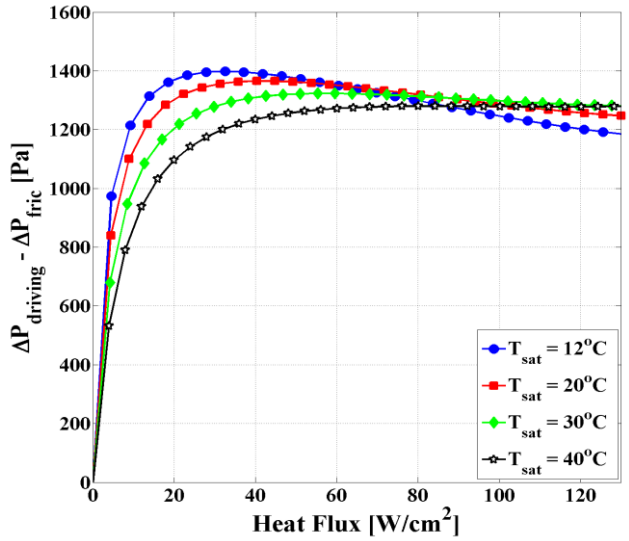

Fig. 4 Simulation of net driving potential as a function of heat flux for $\dot{m}_{ref}$ = 8 kg/hr.

The convective thermal resistances for the results shown in Figure 3 are compared in Figure 5. As expected, the convective thermal resistance was lower for q = 15 – 25 W/cm^2 ($\dot{m}_{water}$ = 10 kg/hr) due to higher refrigerant mass flow but becomes inferior in comparison with $\dot{m}_{water}$ = 8 kg/hr at q = 30 W/cm^2.

Thermal performance: thermosyphon vs. pumped loop

As mentioned earlier, flow boiling data for the pumped loop were also acquired with the aim to provide a quantitative comparison with the thermosyphon closed loop system, although the exact conditions cannot be reproduced.

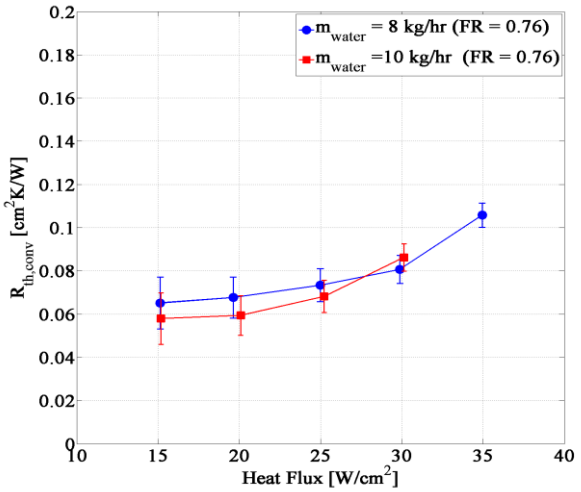

Fig. 5 Micro-evaporator convective thermal resistance (without accumulator) for $T_{water,in}$ = 12 °C.

The experimental data plotted in Figure 6 were acquired for the pumped loop with 525 grams of refrigerant and FR ~ 0.67 for the thermosyphon with in-line accumulator. The reason for operating the accumulator is to enable experiments to be conducted at higher heat fluxes by mitigating two-phase flow in the downcomer and the inlet to the micro-evaporator. This mitigates evaporator inlet pressure and RTD temperature oscillations, thus allowing flow boiling experiments to be performed at higher heat fluxes. Referring to Figure 6, the thermosyphon convective resistance are fairly constant for the range of heat flux tested, averaging between 0.15 – 0.17 cm^{2}K/W. The pumped loop possessed more flexibility for varying the refrigerant mass flow rate from 4 – 10 kg/hr (G_{ref} = 79 – 197 kg/m^{2}s).

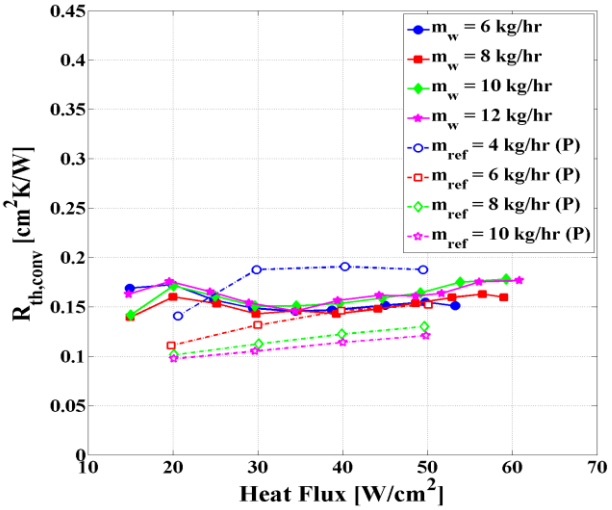

Fig. 6 Comparison of micro-evaporator convective thermal resistance under thermosyphon and pump mode ($T_{water,in}$ = 20 °C and $\dot{m}_{water}$ = 10 kg/hr for the pump mode).

As usual, convective heat transfer has long been known to be associated to the heat and mass fluxes, i.e. higher heat transfer coefficients with increasing heat and mass flux. For the pumped loop, convective thermal resistance increased with decreased mass flux as expected. Referring the Figure 3, the refrigerant mass flux measured for the thermosyphon was only on the order of 3.5 – 5.5 kg/hr. Hence, a comparison of the pumped loop convective resistance at $\dot{m}_{ref}$ = 6 kg/hr for q = 30 - 50 W/cm^2 yielded similar magnitude. As for $\dot{m}_{ref}$ = 4 kg/hr and q = 30 - 50 W/cm^2, the averaged thermal resistance is ~ 25% higher due to increased sub-cooling, ΔT_{sub} = 13 K in comparison with only ΔT_{sub} = 0.25 - 1.0 K for the thermosyphon. This proved that there are no significant benefits of operating a pumped loop with respect to a passive cooled thermosyphon loop from a heat transfer point of view.

The resistance components for the micro-evaporator are depicted in Figure 7. By observation, the average package resistance, i.e. summation of the silicon chip, thermal interface material and copper base resistance are fairly constant for the range of heat flux tested, averaging to ~ 40% of the total resistance. The increase in evaporator's resistance at higher heat loads is attributable to the rise in the convective resistance of the evaporator. At higher heat fluxes, frictional pressure losses become dominant and the refrigerant flow is expected to decrease, resulting in a higher thermal resistance.

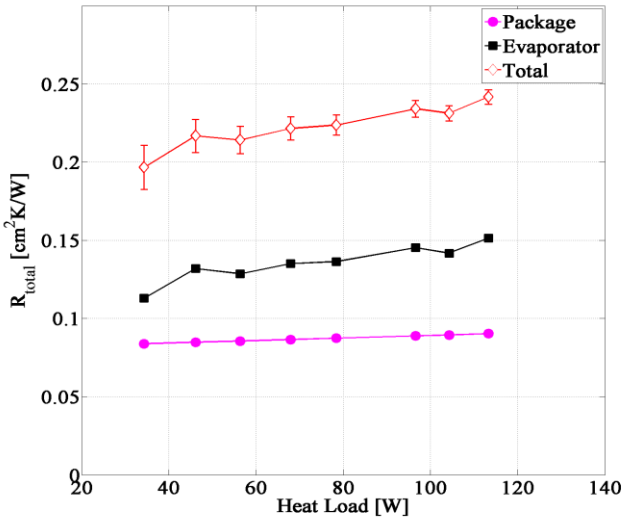

Fig. 7 Micro-evaporator convective and package thermal resistance.

Figure 8 presents the convective heat transfer resistance as a function of heat flux for various condenser cooling water temperatures. Increasing the condenser's water temperature basically yields a higher system saturation pressure/temperature. The first trend observed here is for $T_{water,in}$ = 12 and 16 °C, witnessed by the dramatic rise in thermal resistance with heat flux (more pronounced for $T_{water,in}$ = 12 °C, which must be the gravity dominant region and due to the larger net driving force). The rapid decline in the net driving force for T_{sat} = 12 and 20 °C results in a dramatic decline in coolant flow rate, shown earlier in Figure 3 and explained in Figure 4.

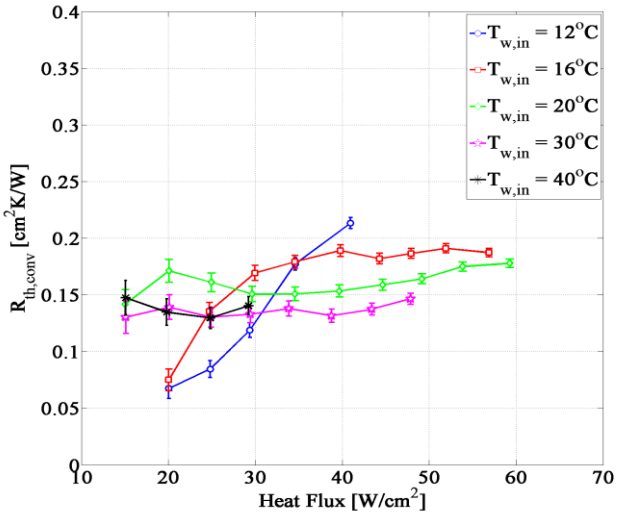

Fig. 8 Micro-evaporator convective thermal resistance for various water inlet temperatures and $\dot{m}_{water}$ = 10 kg/hr (FR ~ 0.67).

At higher water inlet temperatures of $T_{water,in}$ = 30 and 40 °C, a dramatic increase in micro-evaporator inlet pressure is seen (Figure 9). The thermal resistance for these two conditions are somewhat similar in magnitude, the reason being a smaller reduction in net driving force with rising saturation temperature, especially when transiting from 30 – 40 °C, due to lower frictional pressure drop in the downcomer and riser of the thermosyphon loop.

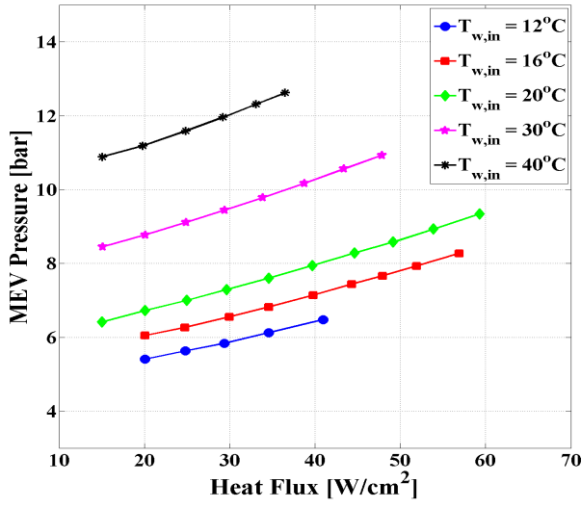

Fig. 9 Micro-evaporator inlet pressure as a function of cooling water temperature.

CONCLUSIONS

A mini-thermosyphon cooling system with a riser height of 15.0 cm has been built and experimentally characterized. The thermal performance characteristics of this thermosyphon loop was shown to be comparable to that of a pumped cooling loop system, demonstrating the feasibility for the eventual design of a smaller and optimized cooling device applicable for server blade cooling, for example a 2U server in Part 4.

Steady-state and transient experimental data (the latter are shown in Part 3) have been acquired during this experimental campaign in addition to the implementation of an innovative non-intrusive mass flow measurement technique to monitor the thermosyphon's refrigerant flow rate. The mass flow measurement results enabled reducing the data as a function of flow rate, to validate the presence of two flow regimes within the loop, namely the GDR and FDR flow regimes, characterized by an ascending and descending mass flow trend with heat flux. With the presence of an in-line accumulator, the thermosyphon was able to sustain stable flow boiling heat transfer for heat loads of up to 137.4 W and q up to 60.9 W/cm^2 (sufficient for existing HPC servers) while still maintaining T_{chip} < 58 °C.

Future experimental work will involve the design and testing of smaller and more compact thermosyphon loops with integrated pressure drop measurements across the riser, condenser and downcomer to yield additional experimental data for the benchmarking and validation of our in-house simulation code, presented in Part 2 and 3 of this study.

ACKNOWLEDGEMENTS

This study is part of the Nano-Tera RTD project YINS financed by the Swiss Confederation and scientifically evaluated by SNSF, which is gratefully acknowledged for the 3 year's post-doctoral support.

REFERENCES

[1] M.J. Ellsworth, Jr. P.E., Thermal design and implementation of robust liquid cooling systems for high performance computer systems, InterPACK'11 Tutorial, U.S.A, 6-8th July 2011.

[2] B. Agostini and M. Habert, Compact thermosyphon heat exchanger for power electronics cooling, Journal of Energy and Power Engineering, Vol.7, pp.972-978, 2013.

[3] A. Rumpunen, Suitability of thermosyphon heat exchanger for cooling of power electronics components, Master Thesis, Aalto University, Finland, 2015.

[4] P.T. Garrity, J.F. Klausner and R. Mei, A Flow Boiling Microchannel Evaporator Plate fir Fuel Cell Thermal Management, Heat Transfer Engineering, Vol.28(10), pp. 877-884, 2007.

[5] J.B. Marcinichen, S. Szczukiewicz, N. Lamaison and J.R. Thome, Towards Development of a Passive Datacenter Cooling Technology: On served Thermosyphon Cooling Loop under Dynamic Workload, 14th IEEE ITHERM Conference, 2014.

[6] M.K. Na, J.S. Jeon and H.Y. Kwak, Experimental Study on Close-Loop Two-Phase Thermosyphon Devices for Cooling MCMs, Heat Transfer Engineering, Vol. 22:29-39, 2001.

[7] C.-C. Chang, S.-C. Kuo, M.-T. Ke and S.-L. Chen, Two-Phase Closed-Loop Thermosyphon for Electronics Cooling, Experimental Heat Transfer, Vol. 23, pp.144-156, 2010.

[8] V. Tsoi, S.W. Chang, K.F. Chiang and C.C. Huang, Thermal Performance of a Plate-Type Loop Thermosyphon at Sub-Atmospheric Pressures, Applied Thermal Engineering Vol.31, pp.2556 - 2567, 2011.

[9] A. Franco and S. Fillippeschi, Experimental Analysis of Closed Loop Two-Phase Thermosyphon (CLTPT) for energy Systems, Experimental Thermal Fluid Science, Vol.51, pp.392-311, 2013.
[10] H. Bieliński and J. Mikielewicz, Chapter 19 - Natural Circulation in Single and Two-Phase Thermosyphon Loop with Conventional Tubes and Minichannels, Heat Transfer, Mathematical Modeling, Numerical Methods and Information Technology, 2011. Weblink: www.intechopen.com